Six-coordinate ruthenium water oxidation catalysts bearing equatorial polypyridinedicarboxylato and axial phosphine ligands

Sima Yazdani, Colton Breyer, Pratibha Kumari, Arnold Rheingold, Rodolphe Jazzar, Guy Bertrand, Douglas Grotjahn

Six-coordinate Ruthenium Water Oxidation Catalysts Bearing Equatorial Polypyridinedicarboxylato and Axial Phosphine Ligands

Sima Yazdani,[†,‡] Colton J. Breyer,[†] Pratibha Kumari,[†,§]Arnold L. Rheingold,[‡] Rodolphe Jazzar,[‡] Guy Bertrand,[‡] Douglas B. Grotjahn*[,†]

† Department of Chemistry and Biochemistry, San Diego State University, 5500 Campanile Drive, San Diego, CA 92182-1030, United States.

‡ UCSD-CNRS Joint Research Laboratory (IRL 3555), Department of Chemistry and Biochemistry, University of California, San Diego, La Jolla, CA 92093-0358, United States

§ Department of Chemistry, Deshbandhu College, University of Delhi, New Delhi-110019, India.

This paper is dedicated to Arnie Rheingold, a dear friend and colleague.

Keywords: Water oxidation, ruthenium, oxygen evolution reaction, carboxylate, phosphine

Abstract: Ruthenium catalysts for water oxidation combining multidentate ligands [2,2′:6′,2″-terpyridine]-6,6″-dicarboxylato (tda) and 2,2'-bipyridine-6,6'-dicarboxylato (bda) with apical phosphine ligands have been prepared. These new complexes were fully characterized by standard spectroscopic and single-crystal X-ray crystallography analyses, and their redox properties were evaluated by electrochemistry. Specifically, [Ru^{II}(tda)(tris(2-furyl)phosphine)$_2$] displayed two reversible redox waves that were assigned to the $Ru^{II/III}$ and $Ru^{III/IV}$ transitions, respectively. The number of turnovers in Ce^{IV}-driven water oxidation reached 258 for the bda analog, and for the tda analog, early reaction rates were first order in initial catalyst concentration. The effects of adding fractional equivalents of Ce^{IV} were studied using UV-vis spectroscopy. Steric and electronic changes in the axial phosphine ligand can exert their effects on the properties and catalytic activity of the resulting complexes, which may be useful when exploring other chemistry of these complexes.

1. Introduction

With the increasing awareness of climate change, the production of a sustainable and eco-friendly energy source is a global challenge. In recent years, much attention has been given to water oxidation as an important half reaction to provide protons and crucially, electrons with which to make hydrogen as a fuel, along with oxygen by-product. In this vein, water oxidation catalysts (**WOC**) have been reported by many groups. Notably, Sun's group [1] designed a mononuclear ruthenium complex [Ru(bda)(isoquinoline)$_2$] (**A**, bda = 2,2'-

bipyridine-6,6'-dicarboxylato) with turnover frequency (TOF > 300 s^{-1}) [1f], meanwhile Llobet's group [2] reported that [Ru(tda-κ-N^3O)$(py)_2$] (**B**, tda = [2,2':6',2"-terpyridine]-6,6"-dicarboxylato) achieved a TOF of 8000 s^{-1} (Scheme 1) [2c]. Meyer's group has performed extensive electrocatalytic investigations on **B** and other systems as well [3]. Homogeneous catalysts can be tuned through variation of ligands and substituents, but we should also note that heterogeneous catalysts have also been intensively studied [4]. Despite these major accomplishments, sustainable catalysis is still impaired by catalyst deactivation in part due to harsh oxidizing reaction conditions. Although degradation pathways are not always fully understood (for a prominent exception, see [3b]), Sun's group has provided some evidence suggesting that loss of axial ligands in **A** occurs [1f], thus motivating the design of more robust catalysts through the manipulation apical coordination sites [1a]. For example, π-extended isoquinolines in **A** as axial ligand substitute for 4-picoline significantly improved catalysis [1f], meanwhile, more systematic investigations of the electronic and noncovalent effects of *N*-bound axial ligands have also been carried by Murata and Concepcion groups respectively [5,6]. The Sun group extended this study to axial *N*-heterocyclic carbene ligands [1k], demonstrating O-O bond formation via water nucleophilic attack (WNA) and a TOF of 0.04 s^{-1}. In line with these studies, a variety of Ru-bda complexes with a different axial ligand containing N, C, S, and O in the first coordination sphere to ruthenium have been reported. Interestingly, analysis of the literature reveals no report on the effect of phosphine apical ligands on WOC catalytic activity [7]. Hence, we wish to report on the preparation of Ru-bda complexes $\mathbf{C^{1-5}}$ and **D** (Scheme 1) and their evaluation in water oxidation processes. $\mathbf{L^{1-5}}$ were chosen to vary the sterics and electronics, and $\mathbf{L^4}$ was chosen to see if the imidazole nitrogen could play a beneficial role under neutral conditions. The question to be addressed was to what extent oxidation catalysis could outrun catalyst (or ligand) degradation.

The complexes were prepared and fully characterized by analytical, spectroscopic (UV-vis and nuclear magnetic resonance (NMR), solid-state monocrystal X-ray diffraction analysis, and electrochemical techniques (cyclic voltammetry and differential pulse voltammetry). Catalytic activity was examined using $Ce(NH_4)_2(NO_3)_6$ (Ce^{IV}) as oxidant. Finally, the catalytic activity of the most efficient catalysts in this study, namely $\mathbf{C^1}$ and **D** bearing the tris(2-furyl)phosphine $\mathbf{L^1}$, is discussed in the light of known pyridine analogues.

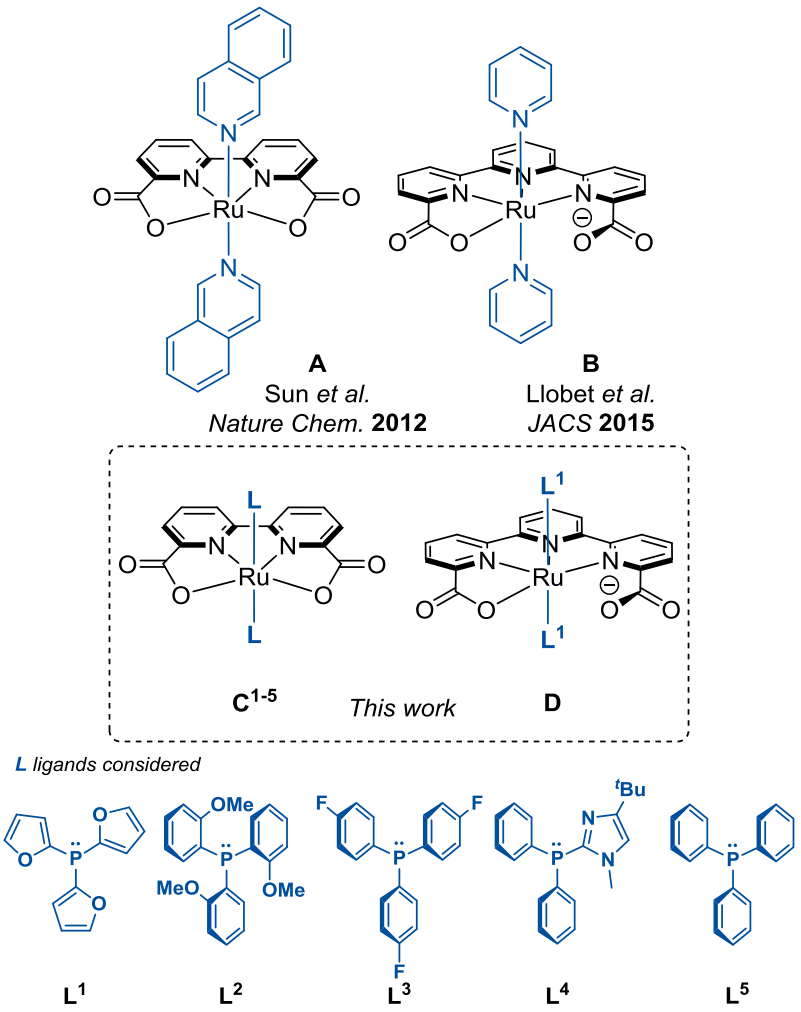

Scheme 1. Known water oxidation catalysts **A** and **B**, and the Ru-bda (**C**) and Ru-tda (**D**) complexes with different phosphorus axial ligands ($\mathbf{L^1}$ – $\mathbf{L^5}$) reported here.

2. Experimental Section

2.1. Materials and Methods

All the synthetic experiments were performed using a standard glovebox and Schlenk line, using commercial-grade solvents and reagents unless otherwise noted. Dichloromethane was freshly distilled over CaH_2 under nitrogen, and methanol was deoxygenated by bubbling nitrogen through it. Deuterium-labeled solvents were purchased from Cambridge Isotope Laboratories and deoxygenated by bubbling nitrogen through them. The Ru-bda and -tda precursors were prepared according to literature [1f, 2, 7]. Multinuclear NMR data were recorded on a Varian INOVA 400 and 500 MHz or a Bruker Avance 300 and 600 MHz spectrometers. Single-crystal X-ray structure determinations were carried out at low temperatures on a Bruker P4, Platform, or Kappa diffractometer equipped with a Mo (λ = 0.710 73 Å) or Cu (λ = 1.541 78 Å) radiation source, and a Bruker APEX detector. Crystals were selected under oil, mounted on nylon loops, and then immediately placed in a cold

stream of nitrogen. All structures were solved by direct methods with SIR 2004 or SHELXS and refined by full-matrix least-squares procedures utilizing SHELXL within the Olex 2 small-molecule solution, refinement, and analysis software package.

2.2. Experimental Procedure

2.2.1 General method for the synthesis of complexes $C^1 – C^5$

A 20 mL scintillation vial in the glove box was charged with Ru(bda)$(DMSO)_2$ (0.1000 g, 0.1994 mmol, 1 equiv) then methanol (5.0 mL) was added. In another vial, the phosphine ligand (0.3988 mmol, 2 equiv) was dissolved in methanol (5 mL), and the resulting solution was added to the vial containing Ru(bda)$(DMSO)_2$. The reaction vial was sealed and the contents stirred at room temperature. The completion of the reaction was monitored with ^{31}P NMR spectroscopy. After completion of the reaction, the mixture was filtered in the glove box, and the filtrate evaporated to dryness. The residue was crystallized either by slow evaporation over time or diffusion using methanol/dichloromethane to produce the desired product.

2.2.2. Procedure for synthesizing complex D

The procedure of Llobet *et al*. [2c] was used for the first step: a 1:1 molar ratio of $RuCl_2DMSO_4$ and H_2tda in Et_3N and dry MeOH was refluxed for 6 hours and cooled to room temperature. A brown solid appeared in the reaction mixture, which was filtered, and washed with methanol and ether [2c]. The resulting solid (which is highly insoluble) was used for the next step without further purification and was assumed to have the formula Ru(tda)$(DMSO)_2$. In the glove box, a 20 mL scintillation vial was charged with the assumed Ru(tda)$(DMSO)_2$ (0.050 g, 0.0996 mmol, 1 equiv), followed by dry methanol (10 mL), resulting in a suspension. Then tris(2-furyl)phosphine) (0.0463 g, 0.1992 mmol, 2 equiv) was added to the suspension, and the mixture was stirred at 70 ^oC for 3 days. The solvents were removed by high vacuum, and the residue was crystallized from methanol (yield 51%, 0.045 g).

3. Results and Discussion

3.1 Preparation, characterization, catalytic behaviour of $C^1 – C^5$

[Ru(bda)$(\mathbf{L^1}$-$\mathbf{L^5})_2$] complexes $\mathbf{C^1} – \mathbf{C^5}$ were readily obtained in good to excellent yield from [Ru(bda)$(DMSO)_2$] [1f, 7], by reacting with two equivalents of the corresponding phosphorus ligand in methanol (Scheme 2). This synthetic strategy allowed us to systematically vary the electronic and the steric properties of the phosphorus ligand.

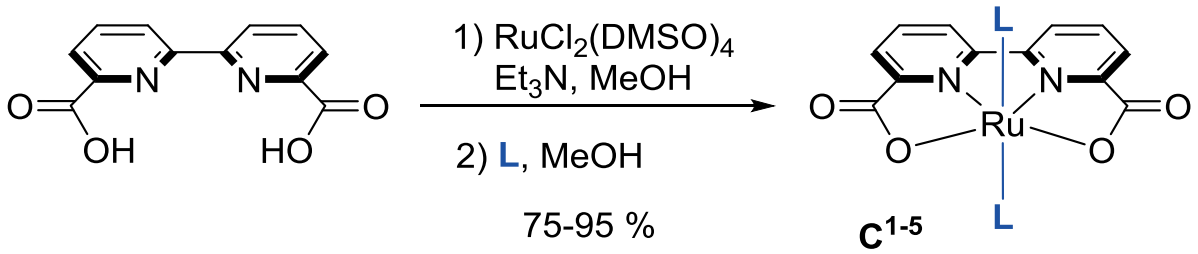

Scheme 2. Synthesis of complexes $\mathbf{C^1}$ – $\mathbf{C^5}$.

We were fortunate to obtain X-ray crystallographic data for $\mathbf{C^1}$ – $\mathbf{C^3}$ (Scheme 3). Of interest, we found that compound $\mathbf{C^1}$ exhibits a O-Ru-O angle that is closer to the angle in **A**, whereas in $\mathbf{C^2}$ and $\mathbf{C^3}$ the angle is slightly larger. Given the respective cone angle for $\mathbf{L^1}$ – $\mathbf{L^3}$ of 133°, 136.6°, and 145° [8], it is likely that the increase in the steric bulk in the apical position cause more distortion in the geometry of these complexes compared to **A** and a wider O-Ru-O angle. It has been proposed that a larger O-Ru-O angle (> 123.1°) is critical to the WOC catalytic activity in allowing the additional coordination in the equatorial plane necessary for the higher oxidation states during the catalysis [1a].

The redox properties of $\mathbf{C^1}$ – $\mathbf{C^5}$ in aqueous solution were assessed via cyclic voltammetry (CV). The CV experiments were performed using glassy carbon working electrodes, a platinum wire as auxiliary, and a silver/silver chloride (Ag/AgCl) as a reference electrode. At pH 7 (phosphate buffer solution), the CV of $\mathbf{C^1}$ shows a chemically reversible peak at $E_{1/2}$ = +0.62 V (ΔE = 80 mV, E_{pa} = 0.66 V) (Figure 1a), assigned to a metal-based one-electron oxidation process [$Ru^{II} \rightarrow Ru^{III}$]. Also clear is catalytic current at pH 7 with onset at approximately +0.9 V. We performed differential pulse voltammetry (DPV) for $\mathbf{C^1}$ to investigate further the redox properties of this complex. In DPV, one oxidation peak is visible in the region of +0.60 V (Figure 1b), which corresponds to the oxidation $Ru^{II} \rightarrow Ru^{III}$ [1]. For $\mathbf{C^1}$, this process occurred at +0.58 V at pH 11.18, at +0.60 at pH 7.07, and at +0.61 at pH 1.99.

Cyclic voltammetry for $\mathbf{C^2}$ - $\mathbf{C^5}$ was conducted in aqueous potassium phosphate (0.1 M, μ = 0.1, pH = 7) (Figure S2). Clear reversible one-electron redox waves for $Ru^{II/III}$ were observed for PPh_3 complex $\mathbf{C^5}$ ($E_{1/2}$ = +0.53 V, E_{pa} = +0.55 V) and $P(4\text{-}FC_6H_4)_3$ complex $\mathbf{C^3}$ ($E_{1/2}$ = +0.63 V, E_{pa} = +0.67 V), with the more positive potential for the fluorinated analog consistent with the electron-withdrawing nature of the ligand. The values of $E_{1/2}$ = +0.62 V, E_{pa} = 0.66 V for $\mathbf{C^1}$ are somewhat surprising, since by looking at both ν_{CO} in $ClRh(L_2)CO$ complexes (Table S1) as well as at $^1J_{PSe}$ in phosphine selenides, $\mathbf{L^1}$ is considered less

electron-donating than $\mathbf{L^3}$ [8a, 8d]. $\mathbf{C^4}$ and $\mathbf{C^2}$ gave less clear CV data (Figure S2). Therefore, in this series of Ru-bda complexes bearing tertiary phosphine axial ligands $\mathbf{C^1}$ – $\mathbf{C^3}$ and $\mathbf{C^5}$, the $Ru^{II/III}$ redox potential shows an increasing trend as $\mathbf{C^5} < \mathbf{C^1} \approx \mathbf{C^3}$.

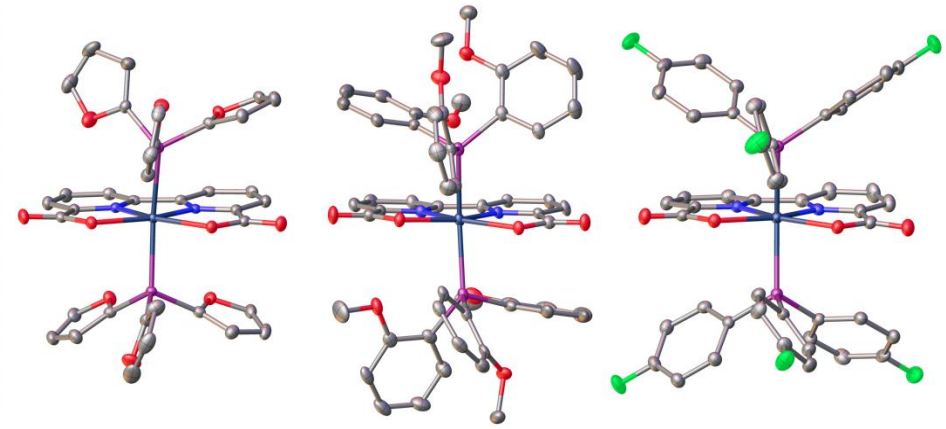

$\mathbf{C^1}$ $\mathbf{C^2}$ $\mathbf{C^3}$

	Bond-Length (Å)			Bond-Angle (°)		
Complex	Ru-O	Ru-N	Ru-P/N	N-Ru-N	O-Ru-O	O-Ru-P/N
$\mathbf{C^1}$	2.190(13) 2.186(13)	1.953(15) 1.954(16)	2.325(5) 2.334(5)	81.43(6)	123.45(5)	88.06(4) 90.39(4)
$\mathbf{C^2}$	2.212(3) 2.207(3)	1.952(3) 1.946(3)	2.411(12) 2.434(12)	81.78(3)	125.50(9)	89.19(8) 81.68(8)
$\mathbf{C^3}$	2.196(18) 2.189(17)	1.952(2) 1.953(2)	2.321(8) 2.369(9)	81.35(9)	124.40(7)	87.19(5) 83.23(5)
A	2.172(6) 2.216(7)	1.949(7) 1.914(6)	2.070(6) 2.084(6)	82.10(3)	123.00(2)	87.40(2) 83.89(2)

[a] Selected bond lengths and bond angles. Hydrogen atoms have been omitted for clarity. Data for A are from reference [1a].

Scheme 3. Solid state structures of **C1** – **C3**.

3.2 Catalytic activity of bda complexes $\mathbf{C^1}$ – $\mathbf{C^4}$ in O_2 evolution

We studied the catalytic activity of $\mathbf{C^1}$ - $\mathbf{C^4}$ for generating O_2 in the presence of Ce^{IV} as an oxidant (Figure 2a and Table S2). For this experiment, aqueous ceric ammonium nitrate (CAN) at the desired concentration was used in a sealed vessel equipped with pressure transducer, and a small volume of solution containing the catalyst was injected (details are provided in supporting information, pages S20-S22). The tris(2-furyl)phosphine complex $\mathbf{C^1}$ outperformed the other Ru catalysts ($\mathbf{C^2}$ - $\mathbf{C^4}$) at similar concentrations, while $\mathbf{C^4}$ led to the lowest performance (Table S2). Our catalytic results in the order $\mathbf{C^1} > \mathbf{C^2} > \mathbf{C^3} > \mathbf{C^4}$ correlates with a higher activity of electron-deficient apical ligands, which is in good

agreement with literature precedents [1f, 2b]. Although complex $\mathbf{C^1}$ shows the highest TON, complex $\mathbf{C^3}$ shows the highest rate in the 30-to-60 sec time range.

Complex $\mathbf{C^3}$ had a higher onset potential and showed minimal catalytic activity compared to $\mathbf{C^1}$ (Figures S2 and 1a). Under the given catalytic conditions in Figure 2a, complex $\mathbf{C^3}$ deactivated in about 2 minutes while complex $\mathbf{C^1}$ lasted more than 10 minutes. Possibly the loss of the bulkier phosphine ligand ($P(4\text{-}FC_6H_4)_3$, $\mathbf{L^3}$) accelerates the degradation of the catalyst (cone angles for $\mathbf{C^1}$ and $\mathbf{C^3}$ = 133° and 145°, Table S1). At the lowest examined concentration of catalyst $\mathbf{C^1}$, 5 μM, a higher catalytic activity was observed for water oxidation; the turnover number was calculated to be 258 (Figure 2b, Table S3) [2g, 10]. To determine the order with respect to $[catalyst]_0$, we measured rates at an early phase of the reaction. Two phases of the oxygen evolution were seen: the first was from t = 0 to a range between t = 12 and 30 sec, in which most of the O_2 was formed. To be consistent, we considered the initial phase to be the first 30 sec. The second phase occurred in the next 30 sec, after injection was finished, from t = 30 to 60 sec. During the first phase there were perturbations due to needle insertion and removal that preclude direct use of the data. To estimate the order with respect to $[\mathbf{C^1}]_0$, we used the second phase, but as shown in Figure 2c, the linear fitting from t = 30 to 60 sec is neither interpretable as first-order nor second-order reaction [1, 2]. Unfortunately, it was not feasible to inject faster while also ensuring all catalyst solution reached the oxidant solution.

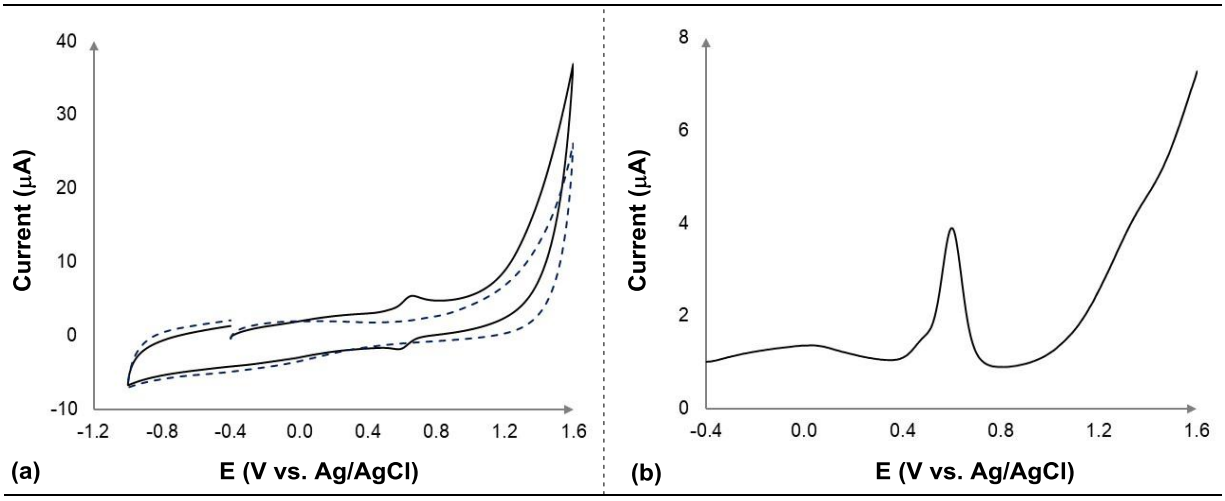

Figure 1. (a) CV of $\mathbf{C^1}$ vs. background (dashed line) in phosphate buffer/CF_3CH_2OH (65:35) solution ([$\mathbf{C^1}$] = 0.32 mM, 0.05 V/s, pH 7, ionic strength 0.1 M). CV demonstrates a reversible redox peak at $E_{1/2}$ = +0.62 V. (b) Plot of DPV of $\mathbf{C^1}$ in phosphate buffer solution (pH 7). Conditions for all the electrochemistry experiments: working electrode, glassy carbon; counter electrode, Pt wire; reference electrode, Ag/AgCl.

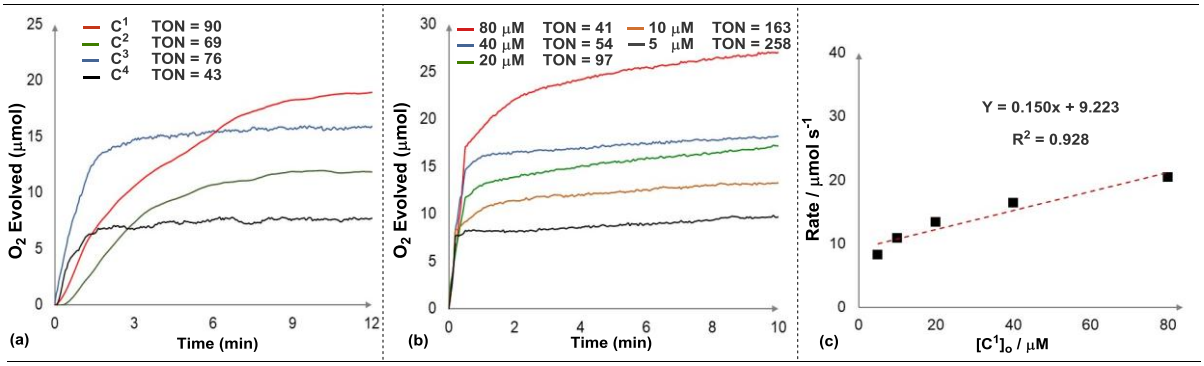

Figure 2. (a) Oxygen evolution catalyzed by **C^1** - **C^4**, $[Cat.]_0$ = 20 µM, in aqueous solution (HNO_3, pH 1, 10 mL) containing $[Ce^{IV}]_0$ = 0.20 M. More details are presented in Table S2; pressure build-up in a sealed cell gave the measurements shown. (b) Oxygen evolution catalyzed by **C^1** in aqueous solution (HNO_3, pH 1, 5.0 mL), with $[Cat.]_0$ ranging from 5 to 80 µM and $[Ce^{IV}]_0$ fixed at 0.21 M (Table 3). (c) The rate of O_2 evolution in the period 30 to 60 sec after first catalyst injection, versus initial concentration of **C^1** (see text).

3.3 Stoichiometric oxidation of C^1 monitored by UV-Vis spectroscopy

Given the catalytic activity observed with **C^1**, we added successive 0.2-equivalent portions of Ce^{IV} oxidant to **C^1** in triflic acid (pH = 1) and observed the UV-vis spectra (Figure 3 and S4c). Figure 3c shows the $[Ce^{IV}]$-dependent absorbances at wavelengths 309 nm and 326 nm, that show clear dependences on amount of Ce^{IV} added. The absorption rises to a maximum at 2 equivalents, suggesting the formation of one or more higher oxidation states.

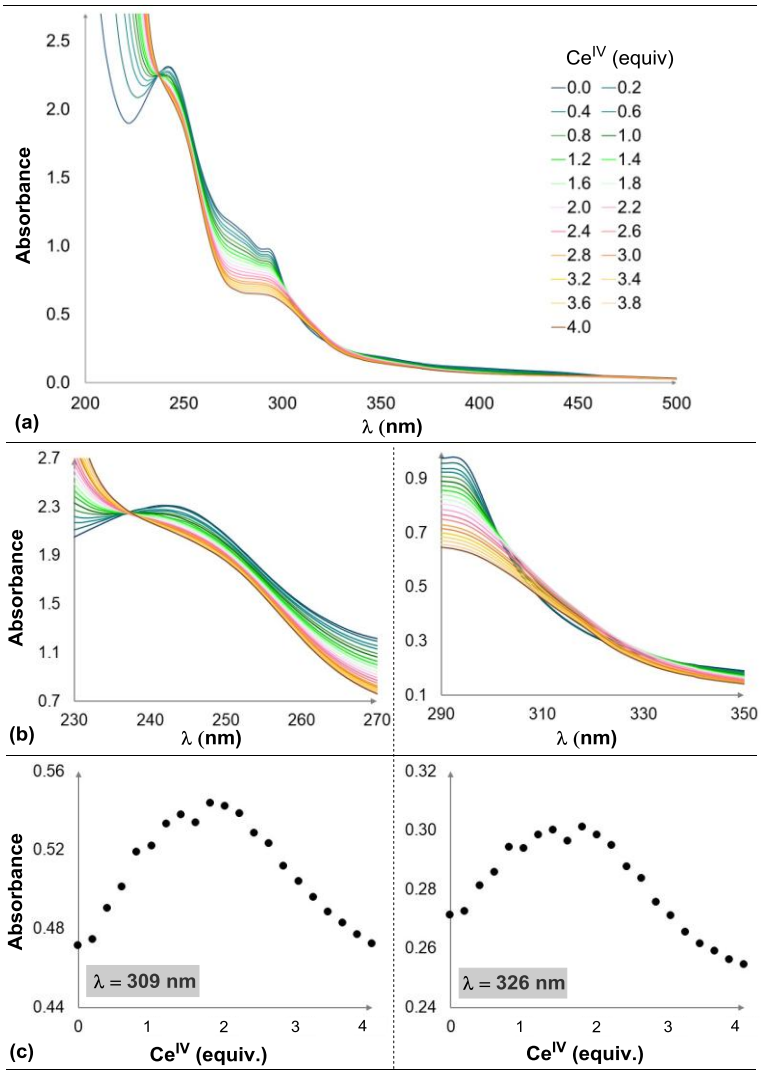

Figure 3. UV-vis spectra of $\mathbf{C^1}$. (a) Spectrophotometric redox titration of $\mathbf{C^1}$ (70 µM) in pH 1 triflic acid (0.1 mM) by CAN (0 to 4 equivalents of CAN, and each time 0.2 equivalent CAN solution added, 1.1 mM stock solution of CAN); (b) Close-up of isosbestic point in the region between 230-270 nm, and second close up of the region 290 - 350 nm; (c) Plot of absorbance against equivalents of CAN at selected wavelengths (309 nm and 326 nm). Wavelengths 246 and 343 nm are presented in SI.

3.4 Preparation, characterization, catalytic behaviour of D

Following upon our results with $\mathbf{C^1}$, we expanded our investigation to a tris(2-furyl)phosphine ($\mathbf{L^1}$) analog of the tda ruthenium catalyst **B**. Consequently, Ru(tda-κ-N_3O)[tris(2-furyl)phosphine]$_2$ **D** was prepared by reaction of [2,2':6',2''-terpyridine]-6,6''-dicarboxylic acid (H_2tda) with $RuCl_2(DMSO)_4$ [2c], followed by ligand exchange with $\mathbf{L^1}$ (Scheme 4).

Scheme 4. Synthesis of [Ru(tda)(tris(2-furyl)phosphine)$_2$] **D**.

Crystallographic analysis of complex **D** reveals a six-coordinate ruthenium center with one carboxylate, which displays the typical disordered octahedral geometry around a low-spin d^6 Ru^{II} in center. The Ru-O distance for the bonded carboxylate is 2.347(17) Å whereas the nonbonded carboxylate is 2.959 Å. Of note, the Ru-N bond distances (ca. 1.948(3) - 2.061(2) - 2.061(2)) in complex **D** are smaller than in the analogous Llobet complex **B** (2.105(2) - 2.114(5) - 2.118(5)) [2c]. Selected bond angles and distances are presented in Scheme 5.

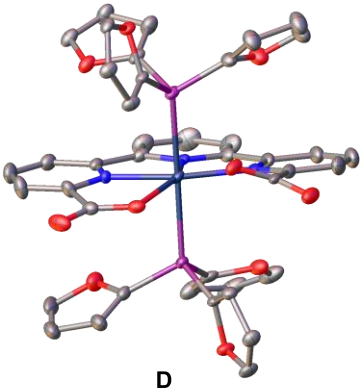

D

	Bond-Length (Å)			Bond-Angle (°)	
Complex	Ru-O	Ru-N	Ru-P/N	N-Ru-N	O-Ru-P/N
D	2.959 2.347(17)	2.061(2) 1.948(3) 2.061(2)	2.3427(6) 2.3427(6)	79.828 79.828	74.110 101.248
B	2.014(4) 2.026(4)	2.105(2) 2.114(5) 2.118(5)	2.108(5) 2.105(5)	72.50(3) 72.02(2)	88.15(18) 86.85(15)

[a] Selected bond lengths and bond angles. Hydrogen atoms have been omitted for clarity. Data for **B** are literature values [2c].

Scheme 5. Solid state structure of **D** and comparison with that of **B**[a].

Turning to electrochemistry, complex **D** shows two reversible redox waves at $E_{1/2}$ = 0.53 V (ΔE = 40 mV) and $E_{1/2}$ = 0.91 V (ΔE = 42 mV) at pH 1 and 0.15 V/s (Figure 4a). To evaluate if the potentials of these waves are pH-dependent, we also performed CV at pH 7. In this case two waves were observed at $E_{1/2}$ = 0.37 V (ΔE = 91 mV) and $E_{1/2}$ = 0.91 V (ΔE = 62 mV) (Figure 4b), which we assigned to two consecutive metal-based one-electron oxidation processes [$Ru^{II} \rightarrow Ru^{III} \rightarrow Ru^{IV}$]. Using 15 CV scans between 0.05 - 1 V/s at pH 7 allowed us to confirm the scan rate dependence for this complex; note that for this experiment, the potential was scanned up to 1.6 V. The plot of the current versus square root of the scan rates is linear which clearly demonstrates that the $Ru^{II/III}$ couple is diffusion controlled (Figure S3 in SI). In this case, as the scan rate was reduced, we noted a progressive growth in normalized current in the 1.1 - 1.6 V region, which we attribute to the kinetic dependency of the catalytic event. In line with Llobet *et al.*, we hypothesized that a more electroactive species was formed at longer time scale [2c]. To verify this hypothesis, up to 333 scans (ν = 0.02 V/s) were performed under similar conditions (Figure 4c). In our case, however, we observed a gradual deactivation of catalyst, as highlighted by a progressive loss in the intensity of the corresponding $Ru^{II} \rightarrow Ru^{III} \rightarrow Ru^{IV}$ transitions. Nonetheless, our electrochemical experiments support for single outer sphere electron transfer processes associated with the $Ru^{II/III}$ and $Ru^{III/IV}$ redox couples [2g]. We next evaluated the catalytic activity of **D** in Ce^{IV} and found that this complex was reaching up to 123 TON (Table S4). The analysis of the O_2 evolution catalyzed by **D** was examined by a series of trials, in which the present concentration of **D** was changed, but the concentration of CAN was kept constant (large excess of Ce^{IV}) (Figure 5). The decay of CAN is insignificant during the catalytic reaction because a large excess of CAN was added. The initial rate of O_2 evolution linearly depends on the concentration of **D**, following a first-order kinetics rate = k_{O2}[**D**]. The first order rate in catalyst concentration (for more information see supporting information), suggests a single-site water nucleophilic attack (WNA) mechanism as interpreted for the analogous catalyst **B** [1f].

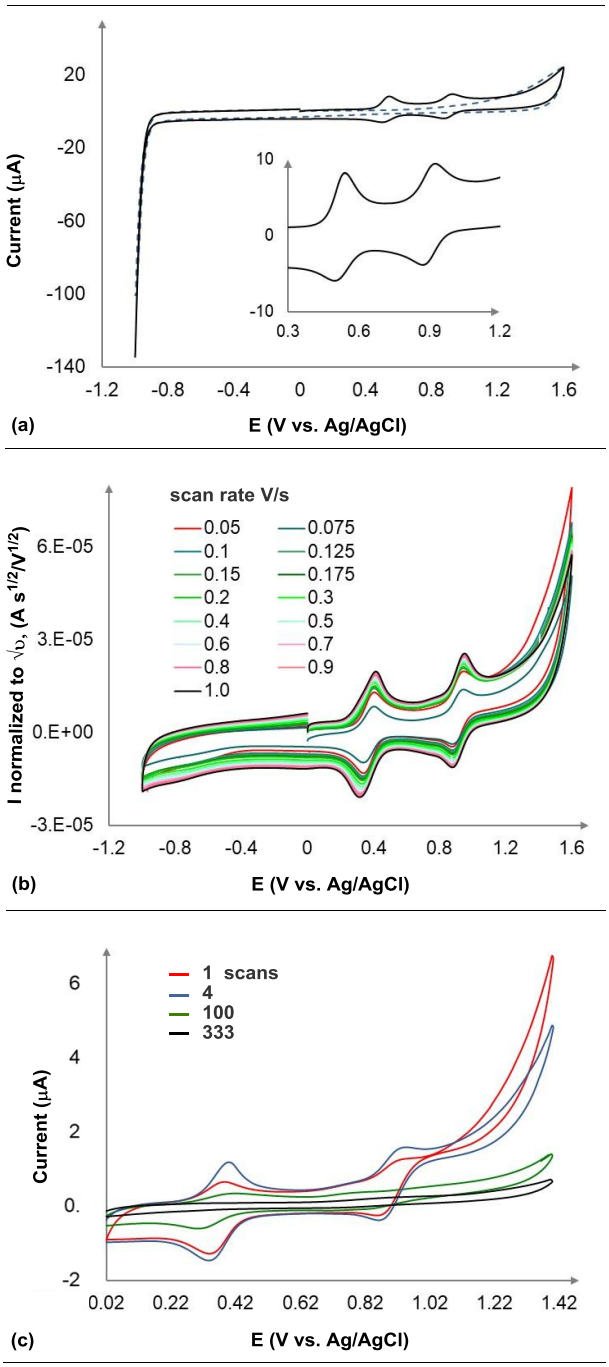

Figure 4. (a) Cyclic voltammetry of **D** (2.6 mM) (black line), in pH 1 aqueous triflic acid solution at a scan rate of 0.15 V/s by using a glassy carbon working electrode (background presented as a dashed line). (b) CV with variable scan rate (0.05 to 1 V/s) of 2.6 mM **D** in pH 7 in phosphate buffer. CVs with current normalized to the square root of the scan rate (ionic strength 0.1 M). (c) Repetitive cyclic voltammetry experiments (ν = 0.02 V/s) in pH 7 phosphate buffer of 1.7 mM of **D**. The red line represents the first scan, the blue line is 4 scans, and finally, the black line shows the last scan with 333 cycles in between. $[\mathbf{D}]_0$ 0.79 mM.

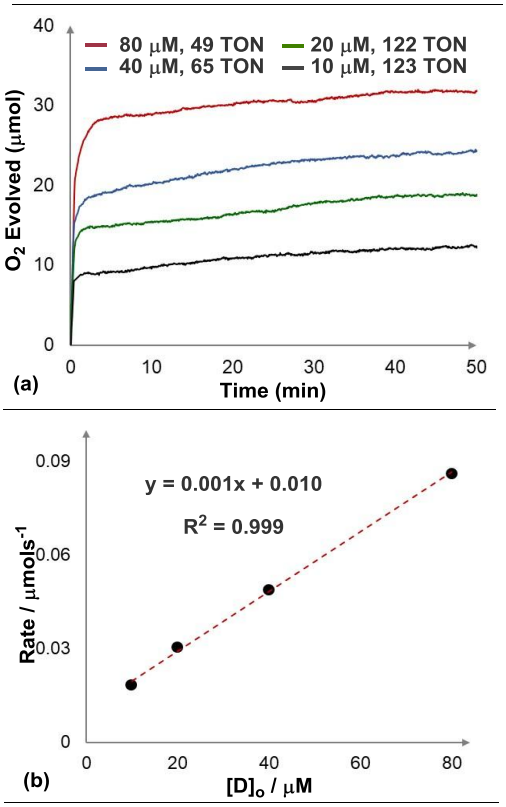

Figure 5. (a) Oxygen evolution catalyzed by **D** in aqueous solution (HNO_3, pH 1, 5.0 mL), $[\mathbf{D}]_0$ variable and containing $[Ce^{IV}]_0$ =0.21 M. (b) The rate of O_2 evolution versus concentration of **D**. The rate is calculated by linearly fitting the post injection O_2 evolution versus time plots in a 50 s period. (More information presented in Figure S5 in SI).

3.4.1 Stoichiometric stepwise oxidation of D monitored by UV-vis spectroscopy

To better understand these results, stepwise oxidation of **D** was conducted with stoichiometric quantities of Ce^{IV} followed by UV-vis and NMR spectroscopies. As previously noted for $\mathbf{C^1}$, by adding up to 4 equivalents of Ce^{IV} (in triflic acid, pH 1; aqueous solution), a direct correlation between the absorption and the concentration of Ce^{IV} is observed. In Figure 6, spectrophotometric redox titration of **D** with Ce^{IV}, shows isosbestic points at 246, 272, 343, and 380 nm. Llobet and co-workers note that typical Ru-bda ruthenium-ligand charge transfer bands appear at wavelengths in 420 - 620 nm range [2c], which for **D** appear 420 - 550 nm until addition of 1 equiv Ce^{IV}.

More interestingly, using 5 equiv of Ce^{IV} resulted in a net decrease of the absorption suggesting the formation of Ru^{III} (Figure S4a in SI). Unsurprisingly, an excess of Ce^{IV} resulted in oxidation of $\mathbf{L^1}$ as confirmed by phosphorus NMR. However, in contrast to

behavior in presence of Ce^{IV}, **D** remains stable in aqueous solution and under an ambient atmosphere for months.

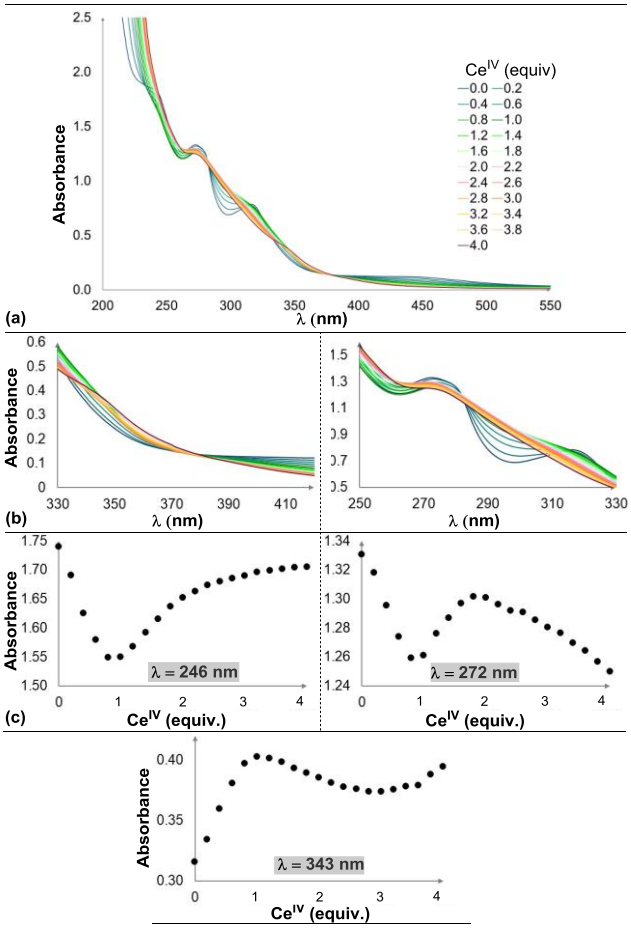

Figure 6. UV-vis spectrum of **D** at pH = 1 in triflic acid (a) Spectrophotometric redox titration of **D** (70 µM) at pH 1 triflic acid (0.1 M) by CAN (0 to 4 equivalents of CAN, and each time 0.2 equivalent CAN solution added, 1.1 mM stock solution of CAN) (b) Close-up of isosbestic point between 330 - 410 nm and 250 - 330 nm (c) Plot of absorbance against equivalents of CAN at selected wavelengths (246, 272, and 343 nm).

Conclusions

In summary, we report a detailed characterization of the spectroscopic, electrochemical, and catalytic properties of related $[Ru(bda)(L)_2]$ and $[Ru(tda\text{-}\kappa\text{-}N^3O)(L)_2]$ complexes containing axial ligands L that are tertiary phosphines. Our study identified that replacing N-containing ligands with more sterically hindered and electron-donating tertiary phosphorus ligands did not significantly affect the geometry of the equatorial plane despite the bulk of the PR_3 ligands. Despite the electrochemistry and kinetic studies, a WOC mechanism could not be established for complex $\mathbf{C^1}$. In the case of **D**, however, first order

rate in catalyst concentration suggests a single-site water nucleophilic attack (WNA) mechanism, also proposed for analogous catalyst **B**. Furthermore, for **D** the $Ru^{II/III}$ couple occurs at 0.37 V followed by the $Ru^{III/IV}$ couple at 0.91 V, and the onset of catalysis begins at ~ 1.3 V. The mechanisms of the catalysts were not studied in further detail, but literature cited already [1,2] provides ample precedent for either water nucleophilic attack on a RuO unit (WNA), or intermolecular coupling of two RuO units (I2M) as likely steps for forming the O-O bond that ultimately becomes molecular oxygen.

Complexes $\mathbf{C^1}$ (TON_{max} = 258) and **D** (TON_{max} = 123) feature axial ligands that are very different than the normal pyridinic type, and they gave rather modest amounts of oxygen when used as catalysts, most likely because of phosphine oxidation, but to fully elaborate the reasons would require a great amount of further investigation. Complexes $\mathbf{C^1}$ - $\mathbf{C^5}$ and **D** are not nearly as robust as benchmark catalysts such as **A** or **B**, but they compare favorably with other attempts to drastically change the axial ligand, such as Ru-bda with *N*-heterocyclic carbene in the axial position ($[Cat.]_0$ = 0.3 μmol, $[Ce^{IV}]_0$ = 0.40 M, TON = 32) [1k]. The results in our report here, along with our previous publication [7], manifest how steric and electronic changes in the axial phosphine ligand can exert their effects on the properties and catalytic activity of the resulting complexes, which may be useful when exploring other chemistry of these complexes.

Accession Codes

CCDC 2010686 − 2010690 contain the supplementary crystallographic data for this paper. These data can be obtained free of charge via **www.ccdc.cam.ac.uk/data_request/cif**, or by emailing **data_request@ccdc.cam.ac.uk**, or by contacting The Cambridge Crystallographic Data Centre, 12 Union Road, Cambridge CB2 1EZ, UK; fax: +44 1223 336033

Declaration of Competing Interest

The authors declare that they have no competing financial interests or personal relationships that could have influenced the work presented in this paper.

Acknowledgments

We thank San Diego State University for initial support of this work by a SDSU University Graduate Fellowship (S.Y.). This research was supported by the U.S. Department of Energy, Office of Basic Energy Science, under Award DE-SC0018310 (Sept. 2017 – Sept. 2024). Authors thank Rebecca Samuels for her contribution in preparing the TOC graphic.

PK is thankful to the Department of Science and Technology (DST), Government of India and the Indo-US Science & Technology Forum (IUSSTF) for her Indo-US Fellowship for women in STEMM.

REFERENCES

[1] (a) A review: B. Zhang, L. Sun, Ru-Bda: Unique Molecular Water-Oxidation Catalysts with Distortion Induced Open Site and Negatively Charged Ligands, J. Am. Chem. Soc. 141 (2019) 5565–5580. (b) Y. Xu, T. Åkermark, V. Gyollai, D. Zou, L. Eriksson, L. Duan, R. Zhang, B. Åkermark, L. Sun, A New Dinuclear Ruthenium Complex as an Efficient Water Oxidation Catalyst, Inorg. Chem. 48 (2009) 2717–2719. (c) L. Duan, A. Fischer, Y. Xu, L. Sun, Isolated Seven-Coordinate Ru(IV) Dimer Complex with [HOHOH]-Bridging Ligand as an Intermediate for Catalytic Water Oxidation, J. Am. Chem. Soc. 131 (2009) 10397–10399. (d) L. Tong, L. Duan, Y. Xu, T. Privalov, L. Sun, Structural Modifications of Mononuclear Ruthenium Complexes: A Combined Experimental and Theoretical Study on the Kinetics of Ruthenium-Catalyzed Water Oxidation, Angew. Chem., Int. Ed. 50 (2011) 445–449. (e) L. Wang, L. Duan, B. Stewart, M. Pu, J. Liu, T. Privalov, L. Sun, Toward Controlling Water Oxidation Catalysis: Tunable Activity of Ruthenium Complexes with Axial Imidazole/DMSO Ligands, J. Am. Chem. Soc. 134 (2012) 18868-18880. (f) L. Duan, F. Bozoglian, S. Mandal, B. Stewart, T. Privalov, A. Llobet, L. Sun, A Molecular Ruthenium Catalyst with Water-Oxidation Activity Comparable to that of Photosystem II, Nature Chem. 4 (2012) 418–423. (g) L. Duan, C. M. Araujo, M. S. G. Ahlquist, L. Sun, Highly Efficient and Robust Molecular Ruthenium Catalysts for Water Oxidation, Proc. Natl. Acad. Sci. USA 109 (2012) 15584–15588. (h) L. Duan, L. Wang, A. K. Inge, A. Fischer, X. Zou, L. Sun, Insights into Ru-Based Molecular Water Oxidation Catalysts: Electronic and Noncovalent-Interaction Effects on Their Catalytic Activities, Inorg. Chem. 52 (2013) 7844–7852. (i) L. Duan, L. Wang, A. K. Inge, A. Fischer, X. Zou, L. Sun, Insights into Ru-Based Molecular Water Oxidation Catalysts: Electronic and Noncovalent-Interaction Effects on Their Catalytic Activities, Inorg. Chem. 52 (2013) 7844–7852. (j) L. Wang, L. Duan, Y. Wang, M. S. G. Ahlquist, L. Sun, Highly Efficient and Robust Molecular Water Oxidation Catalysts Based on Ruthenium Complexes, Chem. Commun. 50 (2014) 12947–12950. (k) R. Staehle, L. Tong, L. Wang, L. Duan, A. Fischer, M. S. Ahlquist, L. Sun, S. Rau, Water Oxidation Catalyzed by Mononuclear Ruthenium Complexes with a 2,2’-Bipyridine-6,6’-

Dicarboxylate (Bda) Ligand: How Ligand Environment Influences the Catalytic Behavior, Inorg. Chem. 53 (2014) 1307–1319. (l) B. Zhang, F. Li, R. Zhang, C. Ma, L. Chen, L. Sun, Characterization of a Trinuclear Ruthenium Species in Catalytic Water Oxidation by Ru(Bda)$(Pic)_2$ in Neutral Media, Chem. Commun. 52 (2016) 8619–8622. (m) Q. Daniel, L. Duan, B. J. J. Timmer, H. Chen, X. Luo, R. Ambre, Y. Wang, B. Zhang, P. Zhang, L. Wang, F. Li, J. Sun, M. Ahlquist, L. Sun, Water Oxidation Initiated by in Situ Dimerization of the Molecular Ru(Pdc) Catalyst, ACS Catal. 8 (2018) 4375–4382.

[2] Two reviews: (a) R. Matheu, P. Garrido-Barros, M. Gil-Sepulcre, M. Z. Ertem, X. Sala, C. Gimbert-Suriñach, A. Llobet, The Development of Molecular Water Oxidation Catalysts, Nature Rev. Chem. 3 (2019) 331–341. (b) R. Matheu, M. Z. Ertem, C. Gimbert-Suriñach, X. Sala, A. Llobet, Seven Coordinated Molecular Ruthenium-Water Oxidation Catalysts: A Coordination Chemistry Journey, Chem. Rev. 119 (2019) 3453–3471. Key papers: (c) R. Matheu, M. Z. Ertem, J. Benet-Buchholz, E. Coronado, V. S. Batista, X. Sala, A. Llobet, Intramolecular Proton Transfer Boosts Water Oxidation Catalyzed by a Ru Complex, J. Am. Chem. Soc. 137 (2015) 10786–10795. (d) M. Gil-Sepulcre, M. Böhler, M. Schilling, F. Bozoglian, C. Bachmann, D. Scherrer, T. Fox, B. Spingler, C. Gimbert-Suriñach, R. Alberto, R. Bofill, X. Sala, S. Luber, C. J. Richmond, A. Llobet, Ruthenium Water Oxidation Catalysts Based on Pentapyridyl Ligands, ChemSusChem 10 (2017) 4517–4525. (e) R. Matheu, M. Z. Ertem, C. Gimbert-Suriñach, J. Benet-Buchholz, X. Sala, A. Llobet, Hydrogen Bonding Rescues Overpotential in Seven-Coordinated Ru Water Oxidation Catalysts, ACS Catal. 7 (2017) 6525–6532. (f) R. Matheu, M. Z. Ertem, M. Pipelier, J. Lebreton, D. Dubreuil, J. Benet-Buchholz, X. Sala, A. Tessier, A. Llobet, The Role of Seven-Coordination in Ru-Catalyzed Water Oxidation, ACS Catal. 8 (2018) 2039–2048. (g) R. Matheu, J. Benet-Buchholz, X. Sala, A. Llobet, Synthesis, Structure, and Redox Properties of a Trans-Diaqua Ru Complex That Reaches Seven-Coordination at High Oxidation States, Inorg. Chem. 57 (2018) 1757–1765. [h] M. Gil-Sepulcre, J. O. Lindner, D. Schindler, L. Velasco, D. Moonshiram, O. Rüdiger, S. DeBeer, V. Stepanenko, E. Solano, F. Würthner, A Llobet, Surface-Promoted Evolution of Ru-bda Coordination Oligomers Boosts the Efficiency of Water Oxidation Molecular Anodes, J. Am. Chem. Soc. 143 (2021) 11651-11661.

[3] (a) N. Song, J. J. Concepcion, R. A. Binstead, J. A. Rudd, A. K. Vannucci, C. J. Dares, M. K. Coggins, T. J. Meyer, Base-Enhanced Catalytic Water Oxidation by a Carboxylate-Bipyridine Ru(II) Complex, Proc. Natl. Acad. Sci. USA 112 (2015) 4935–4940. (b) S.

Neudeck, S. Maji, I. López, S. Meyer, F. Meyer, A. Llobet, New Powerful and Oxidatively Rugged Dinuclear Ru Water Oxidation Catalyst: Control of Mechanistic Pathways by Tailored Ligand Design, J. Am. Chem. Soc. 136 (2014) 24–27. (c) Z. Chen, J. J. Concepcion, H. Luo, J. F. Hull, A. Paul, T. J. Meyer, Nonaqueous Catalytic Water Oxidation, J. Am. Chem. Soc. 132 (2010) 17670–17673.

[4] Examples from the heterogeneous catalysis field, suggested by a reviewer: (a) Y. Pan, R. Abazaei, Y. Wu, J. Gao, Q. Zhang, Review on advances in metal-organic frameworks and their derivatives for diverse electrocatalytic applications, Electrochem. Commun. 126 (2021) 107024. (b) X. Luo, R. Abazari, M. Tahir, W. K. Fan, A. Kumar, T. Kalhorizadeh, A. M. Kirillov, A. R. Amani-Ghadim, J. Chen., Y. Zhou, Trimetallic metal-organic frameworks and derived materials for environmental remediation and electrochemical energy storage and conversion, Coord. Chem. Rev. 461 (2022), 214505

[5] Y. Sato, S. Y. Takizawa, S. Murata, Substituent Effects on Physical Properties and Catalytic Activities toward Water Oxidation in Mononuclear Ruthenium Complexes, Eur. J. Inorg. Chem. 2015 (2015) 5495–5502.

[6] (a) D. W. Shaffer, Y. Xie, D. J. Szalda, J. J. Concepcion, Manipulating the Rate-Limiting Step in Water Oxidation Catalysis by Ruthenium Bipyridine-Dicarboxylate Complexes, Inorg. Chem. 55 (2016) 12024–12035. (b) Y. Xie, D. W. Shaffer, J. J. Concepcion, O-O Radical Coupling: From Detailed Mechanistic Understanding to Enhanced Water Oxidation Catalysis, Inorg. Chem. 57 (2018) 10533–10542.

[7] S. Yazdani, B. E. Silva, T. C. Cao, A. L. Rheingold, D. B. Grotjahn, X-Ray Crystallography and Electrochemistry Reveal Electronic and Steric Effects of Phosphine and Phosphite Ligands in Complexes $Ru^{II}(\kappa^4\text{-bda})(PR_3)_2$ and $Ru^{II}(\kappa^3\text{-bda})(PR_3)_3$ (bda = 2,2’-bipyridine-6,6’- dicarboxylato), Polyhedron 161 (2019) 63–70.

[8] (a) N. G. Andersen, B. A. Keay, 2-Furyl Phosphines as Ligands for Transition-Metal-Mediated Organic Synthesis, Chem. Rev. 101 (2001) 997–1030. (b) Z. L. Niemeyer, A. Milo, D. P. Hickey, M. S. Sigman, Parameterization of Phosphine Ligands Reveals Mechanistic Pathways and Predicts Reaction Outcomes, Nature Chem. 8 (2016) 610–617 (c) J. A. Bilbrey, A. H. Kazez, J. Locklin, W. D. Allen, Exact Ligand Cone Angles, Comput. Chem. (2013) 1189–1197. (d) A. Roodt, S. Otto, G. Steyl, Structure and Solution Behaviour of Rhodium(I) Vaska-type Complexes for Correlation of Steric and Electronic Properties of Tertiary Phosphine Ligands, Coord. Chem. Rev. 245 (2003) 121-137.

[9] Z. Codolà, L. Gómez, S. T. Kleespies, L. Que, M. Costas, J. Lloret-Fillol, Evidence for an Oxygen Evolving Iron-Oxo-Cerium Intermediate in Iron-Catalysed Water Oxidation, Nature Commun. 6 (2015) 5865.

[10] (a) J. M. Kamdar, D. C. Marelius, C. E. Moore, A. L. Rheingold, D. K. Smith, D. B. Grotjahn, Ruthenium Complexes of 2,2′-Bipyridine-6,6′-Diphosphonate Ligands for Water Oxidation, ChemCatChem 8 (2016) 3045–3049 (b) J. M. Kamdar, D. B. Grotjahn, An Overview of Significant Achievements in Ruthenium-Based Molecular Water Oxidation Catalysis, Molecules 24 (2019) 494.